ELSEVIER

J. Non-Newtonian Fluid Mech. 103 (2002) 123–139

Journal of Non-Newtonian Fluid Mechanics

www.elsevier.com/locate/jnnfm

Non-Newtonian effects on ribbing instability threshold

F. Varela López [a,*,1], L. Pauchard [a], M. Rosen [b], M. Rabaud [a]

[a] *Laboratoire FAST, Bât. 502, Campus Universitaire d'Orsay, F91405 Orsay, France*
[b] *Grupo Medios Porosos, Fac. de Ingeniería, UBA, Paseo Colón 850, C1063ACV Buenos Aires, Argentina*

Received 26 January 2001; received in revised form 18 April 2001

Abstract

Threshold of ribbing in a two-roll setup is investigated for non-Newtonian fluids. Two typical shear-thinning polymeric solutions are used, the first one exhibiting inelastic properties (Xanthan), the second one viscoelastic properties (polyacrylamide, PAAm).

The effect of polymeric concentration and thus rheological parameters on the effective critical capillary number Ca^* at the onset of ribbing is described. For low polymer concentrations, only a small decrease of the onset is observed for both fluids. At larger concentrations, Ca^* remains constant for inelastic fluids, while for the elastic fluids, a continuous decrease up to a factor 10, with respect to the Newtonian case, is observed. Above threshold, a strong effect on elastic properties is also observed on the amplitude of ribbing.

Keywords: Threshold; Non-Newtonian effects; Polymer concentrations; Instability

1. Introduction

Ribbing instability has been largely studied both experimentally and theoretically since the early 1960s [1–3] and a review of coating flows and its instabilities can be also found in [4]. The way a planar interface leads to a well-defined, patterned surface above a certain threshold gives rise to detailed research in various fields, from the photographic industry to lubrication of bearings and roll coating processes. In all cases, its industrial importance cannot be overestimated.

Many authors have largely discussed the destabilization mechanism of the ribbing instability (see for example [5]). For the case of Newtonian fluids, linear stability analysis has shown that it can be described by amplitude equations, where control parameter turns out to be capillary number $Ca = \mu V/\sigma$, where μ and σ are the dynamical viscosity and surface tension, respectively, of the fluid, V being the velocity of the moving surface. Linearization around the critical point gives rise to dispersion relation of the unstable

* Corresponding author.
E-mail address: varela@fast.u-psud.fr (F. Varela López).
[1] Associated with Universités Pierre & Marie Curie and Paris-Sud and with CNRS, UMR 7608.

0377-0257/02/$ – see front matter
PII: S0377-0257(01)00165-3

modes and to marginal stability curves, having a well-defined scenario where this instability takes place and evolves as the control parameter increases [6].

Nevertheless, although most industrial fluids (paints, agroalimentary fluids) are known to be non-Newtonian, the effects of rheological properties on coating instabilities have been less studied and complete experimental results are still missing, as can be seen in the review of non-Newtonian coating flows by Chen [7]. Journal bearing flow with non-Newtonian liquids has been well studied, especially in the field of lubrication. Viscoelastic journal bearing flow has been studied using a perturbation technique that leads to several analytical results [8]. Davies and Walters [9] (for the ordered fluids), as well as Phan-Thien and Tanner [10] (for the Criminale–Ericksen–Filbey constitutive relation), predicts the effect of viscoelasticity on load and they also sketch a method for first normal stress measurements using journal bearings. The related problem of parabolic slider lubrication (roll-plate geometry), for shear-thinning fluids has been studied by Sinha and Singh [11], in order to predict load forces and pressure profiles. Dien and Elrod [12], as well as Johnson and Mangkoesoebroto [13] (who improved earlier calculations for the case of negative pressure gradients), studied the problem in a more general context under lubrication approximation, rendering the same results. They found that, as the shear-thinning effect becomes more important, the load decreases and the pressure gradient smoothes out. Greener and Middleman [14] studied theoretically the effect of power-law fluids on pressure distribution along the gap between cylinders. Coyle et al. [15] also found some numerical results on the effect of shear-thinning effects on film thickness. Both papers agree that film thickness increases due to pressure drop in the flow, while the first extend the analysis to viscoelastic fluids, showing that the increase in load (and thus reduction in film thickness) can be masked out by viscosity drop. It must be noted that Greener and Middleman [14] uses a rather ad hoc constitutive relation for its purpose. Ro and Homsy [16] predicted viscoelastic destabilizing effects due to positive normal stress differences on diverging channels, by introducing changes in boundary conditions at the interface.

Experimental results on coating flows with non-Newtonian fluids are rare, possibly because many experimental research is directly involved with industrial research and development. Focusing on base flow, Benkreira et al. [17] measure film thickness at the exit of a two-roll system, showing only a small increase due to shear-thinning effects. Non-Newtonian ribbing instability has been also studied experimentally by some authors. Baumann et al. [18] experimentally found that viscoelastic effects are responsible for an important reduction on threshold instability, according to them due to elongational effects. Fernando and Glass [19] conducting experiments with solutions that differs in extensional viscosity (but not in shear viscosity) found that not only ribbing threshold is reduced, but also the wavelength of the pattern. In the recent years, Dontula et al. [20] found destabilizing effects working with viscoelastic fluids in forward two-roll coating device. Contrarily to the results obtained by Fernando and Glass, extensional viscosity seems to have little influence on ribbing threshold. Grillet et al. [21] described an interfacial instability between two concentric or non-concentric cylinders with constant viscosity elastic fluids. The observed instability is very similar to the one to be presented in this paper, showing threshold reduction and a peaked patterned interface. However, as they work with a large gap, gravity effect plays an important stabilizing role which is not observed in our experiments.

All these studies provide strong evidence that rheological effects, especially viscoelasticity, plays a major role on the development and onset of this hydrodynamic instability. In order to study the effect of rheology on ribbing, we will use two families of polymeric solutions, with a similar shear-thinning behavior but a significant difference in normal stresses. It is the aim of this work to investigate experimentally this influence, characterizing the transition from Newtonian to non-Newtonian behavior by increasing polymer concentration.

2. Experimental setup

Usually, in industrial roll coating, a liquid film flows between two rotating rollers. In order to observe precisely the meniscus shape and thus the onset of instability, our experimental setup consists of a pair of eccentric cylinders one inside the other (journal bearing geometry), as shown in Fig. 1a, and is the same geometry previously used by Bellon et al. [6]. Both cylinders are made of Pyrex and machined with a precision of 0.01 mm. The outer cylinder has an outer radius $R_o = 50$ mm and a length of 420 mm, while the inner one has a radius $R_i = 33$ mm and a length of 380 mm. Such long cylinders allow observation far from the boundaries where end recirculations could be important. The gap between the two rolls, b_0, is adjustable, with a precision of 0.01 mm. In the present work, inner cylinder velocity is the only control parameter. Outer cylinder speed is fixed at a much lower, positive value of 0.8 mm/s. Indeed, the outer cannot be at rest. If it would be the case, since the polymeric solutions are partially wetting, a triple line would be attached to the surface of the cylinder, drastically modifying meniscus position and instability threshold.

An effective curvature can be defined for the journal bearing geometry as

$$\frac{1}{R} = \frac{1}{R_i} - \frac{1}{R_o}.$$

The length R in this case corresponds to the radius of a plane–cylinder system sharing the same curva-

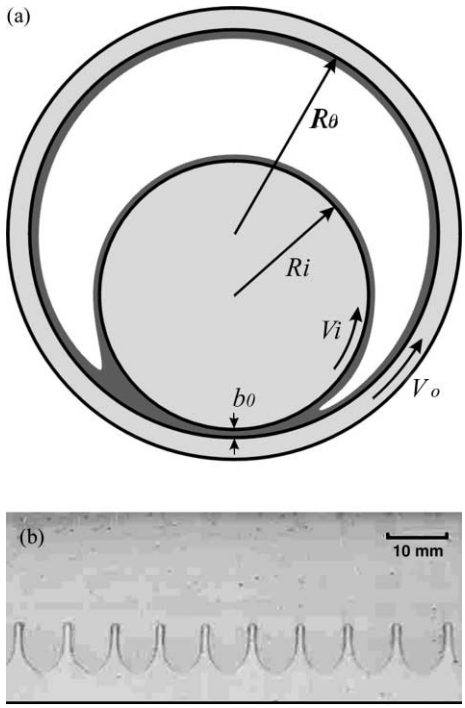

Fig. 1. (a) Sketch of the two-roll setup. $R_i = 33$ mm, $R_o = 50$ mm. Roll spacing b_0 can be adjusted with a precision of 0.01 mm; (b) picture of the meniscus above threshold for a 1000 wppm Xanthan solution. Air is on top, and the bottom line corresponds to minimum gap position ($b_0 = 0.4$ mm, $Ca = 0.38$ and $V_i = 160$ mm/s).

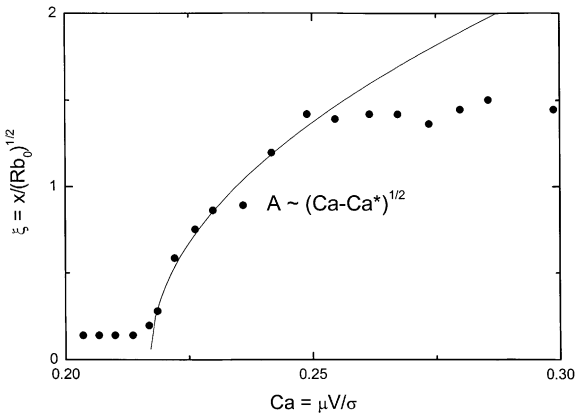

Fig. 2. Evolution of the dimensionless amplitude of the deformation of the interface as observed vs. the capillary number in the case of a Newtonian fluid (glycerol/water solution, $\mu = 105$ mPa s, $\sigma = 54$ mPa m) for a gap $b_0 = 0.4$ mm and fitted by Eq. (1), with $\alpha = 0.5$.

ture. Together with b_0, R defines the geometrical aspect ratio $\Gamma = b_0/R$ and longitudinal length scale $\Lambda = \sqrt{Rb_0}$. In our experimental setup $R = 97.1$ mm, and Γ varied from 5×10^{-4} to 10^{-2}.

In the journal-bearing geometry, meniscus position is a function of velocities of cylinders. If the volume of liquid present in the cell is below certain value, some starvation problems may arise [22]. To avoid this, the volume injected to the system was set equal to 50 cm^3 in all cases. Data acquisition was made by direct visualization through the gap of the air/liquid interface, by means of a CCD camera. In this way the complete wave form could be determined (Fig. 1b). More details about this setup and behavior of Newtonian fluids can be found in [23].

Threshold of instability always presents subtleties and is very difficult to derive an objective method for its determination. Coyle et al. [24] show how different approaches can lead to different results. The method employed in this work is the determination of amplitude of ribs as a function of *Ca* in the vicinity of threshold (Fig. 2). The value of amplitude is given by image analysis via meniscus position recording. Amplitude is then fitted by a power-law:

$$A \propto (Ca - Ca^*)^{\alpha}. \tag{1}$$

From this fit, the critical capillary number Ca^* and the exponent α are extracted. For the case of supercritical instability α is known to be 0.5, considering a single wave number whose amplitude follows the Landau equation [25].

The fluids used for the present experiments were polymeric solutions in an 85/15 wt.% glycerol/water mixture, in order to get a higher viscosity of the solvent phase ($\mu_{sol} = 0.1$ Pa s at 23 °C). This large viscosity slows down the dewetting of the liquid from the slowly rotating outer cylinder. Glycerol mixtures have the disadvantage of having a highly temperature-dependent viscosity, thus all experiences were held in a temperature-controlled room at $T = 23 \pm 0.5$ °C.

Two polymers were tested: the first one is a rigid rod-like polymer (Xanthan Sigma, molar weight $M_w \sim 2 \times 10^6$), while the second is a long flexible polymer (polyacrylamide (PAAm) Floerger AP45, $M_w \sim 12 \times 10^6$). Both showed shear-thinning behavior but only the second exhibits large elastic effects. Special care must be taken while working with ionic polymers, such as Xanthan, in order to get rid of

ionization effects on viscosity, which may cause a rheological bias in viscosity as concentration increases [26]. Indeed, the increase of polymer concentration introduces changes in the electrostatic interaction between the polymer molecule and the solvent. For that reason NaCl was added to the solvent in a concentration of 0.4 M in order to neutralize polymer molecules. This procedure has not been followed for the PAAm solutions, since the molecules are non-polar. Rheology of both solutions is presented in Section 3.

3. Rheology and interfacial properties

The shear viscosity, the first normal stress difference and the surface tension of these solutions have been investigated for various concentrations. This work has been done in stationary conditions, as extensive unsteady measurements, even if there are useful to determine the characteristic time scales of the fluids, were beyond the scope of present work.

3.1. Apparent shear viscosity

Polymeric solutions used in this work were tested with a cone-plate Stress-Tech rheometer under stress-controlled conditions, which allowed measure of viscosity and normal force simultaneously. Viscosities ranged from 4 Pa s to several viscosity values for 1000 wppm in both cases.

For Xanthan, the evolution of the apparent shear viscosity is plotted versus the shear rate for different concentrations C (Fig. 3a). Fig. 3b presents the same plot for the PAAm solutions. Such curves are typical of shear-thinning fluids where a constant Newtonian low-shear viscosity is followed by a power-law dependence before reaching the viscosity of the solvent at high shear. In all cases, the curves can be reasonably fitted by a four-parameter Carreau model [27]:

$$\mu(\dot{\gamma}) = \mu_\infty + \frac{\mu_0 - \mu_\infty}{(1 + (\tau\dot{\gamma})^2)^{p/2}}. \tag{2}$$

$\dot{\gamma}$ is the shear rate, μ_0 and μ_∞ the low and high shear Newtonian viscosities, respectively. The parameter τ is a characteristic time scale, that measures the scale at which shear-thinning effects becomes important. The exponent p takes into account the power-law behavior at intermediate shear rates ($\mu_\infty \ll \mu(\dot{\gamma}) \ll \mu_0$). This model has been widely used especially when a good description of the viscosity is needed under very changing shear conditions [28], as in our case. These fits are shown in Fig. 3 and the parameters of the fit are given in Table 1 (note that the high shear viscosity has always been fixed to the solvent viscosity, thus $\mu_\infty = \mu_{\text{sol}}$). By interpolation of the data of this table, we have good description of the apparent viscosity for any concentration and shear rate. As will be shown in Section 3.2, this is necessary for a correct definition of the control parameter Ca for the case of shear-dependent fluids. A direct correlation can be made between Carreau and Ostwald power-law model by neglecting μ_∞ and identifying $(-p)$ with exponent $(n-1)$ and $\mu_0\tau^{-p}$ with constant k: $\mu = k\gamma^{n-1}$. However, in our experiments, shear rates up to 200 s^{-1} were achieved, for that reason the Ostwald model does not describe the apparent viscosity of the polymeric solutions studied accurately enough.

The intrinsic viscosity $[\eta_0]$, as described in [29], is a measure of molecular effective size, that can be obtained from low-shear viscosity measurements. In this way, different solutions can be compared, putting in evidence the transition from dilute trough a semi-diluted regime. In the case of Xanthan, $[\eta_0] = 6 \times 10^{-3}\,\text{wppm}^{-1}$, while for PAAm $[\eta_0] = 2.1 \times 10^{-3}\,\text{wppm}^{-1}$. Despite its lower molecular weight,

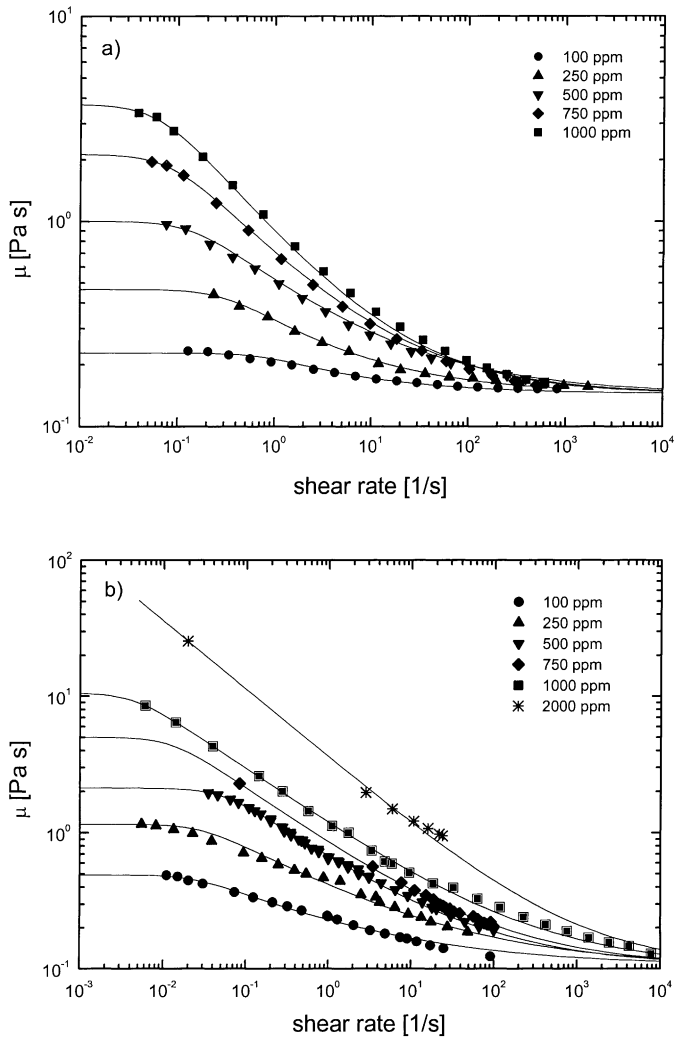

Fig. 3. Log–log plot of the apparent shear viscosity vs. the shear rate $\dot{\gamma}$ for (a) Xanthan solutions and (b) PAAm solutions.

Xanthane solutions presents a much higher intrinsic viscosity than PAAm, since it is a rigid polymer, having a higher effective volume fraction. However, it seems that in the case of PAAm this value might be underestimated considering the shear-thinning effects present at concentrations below semi-dilute limit.

3.2. Normal stress

We measured also the first normal stress difference N_1 defined as

$$N_1 = \tau_{xx} - \tau_{yy}, \tag{3}$$

where τ_{xx} and τ_{yy} are the normal components of the stress tensor parallel and transverse to the flow, respectively. This normal stress was measured by two techniques: first with the rheometer in the cone/plane

Table 1
Coefficients of the Carreau law for Xanthan and PAAm solutions, $\mu_\infty = 0.1$ Pa s

	μ_0 (Pa s)	τ (s)	p
Xanthan (ppm)			
100	0.23	1.24	0.43
250	0.47	3.3	0.44
500	1.09	7.1	0.46
750	2.13	11.8	0.51
1000	3.70	16	0.56
PAAm (ppm)			
100	0.49	43	0.30
250	1.2	35	0.34
500	2.1	20	0.42
750	5.0	78	0.39
1000	11	226	0.40

geometry by measuring the vertical force applied on the cone [28]. The second method follows from the fact that elastic fluids present a swell when a jet of liquid drains from a small tube [30,31]. From these die swell measurements it is possible to deduce the value of N_1 particularly for large shear rates. While for Xanthan this value remains very small for the whole range of shear rates and concentrations (<10 Pa), PAAm showed a significant N_1 value even for the lowest concentrations (>100 wppm) (Fig. 4a). First normal stress coefficient $\Psi_1 = N_1/\dot{\gamma}^2$ can be calculated from this data, remaining almost constant over a wide range of shear rates. This is in agreement with predictions for semi-dilute polymer solutions [28]. N_1 has also been measured as a function of reduced polymer concentration, at a constant shear rate of $200\,s^{-1}$, close to the onset values (Fig. 4b). These results exhibit strong elastic effects in these solutions, which will play an important role on the ribbing threshold, as will be seen in Section 4. From Fig. 4, a characteristic time scale for each fluid can be defined via first normal stress coefficient: $\Psi_1 = \mu_0\lambda$ (assuming a constant Ψ_1, as predicted for example in the upper convected Maxwell model [32]). From this, a Deborah number can be estimated:

$$De = \lambda\Omega, \tag{4}$$

where Ω is the angular frequency of the inner cylinder. This number gives an estimate of the influence of relaxation time on the flow. In the case of PAAm, *De* is about 10^{-2} to 10^{-1}. The time scale of stress variations imposed to the fluid particles is long with respect to elastic time scale. Thus, one can assumes that the fluid is always in equilibrium with local flow conditions, and that time-dependent effects are not relevant. Similar criteria [10] have been employed to define the validity of several non-relaxing constitutive equations on journal-bearing geometry. Weissemberg number can be defined as well: $We = \lambda\dot{\gamma}$, which measures the strength of elastic effects in the flow. A small *De* does not necessarily means small *We*. In fact they are both related with geometrical aspect ratio, i.e. $De \sim \Gamma\, We$, and since Γ is of order 10^{-3}, *We* varies between 10 and 100. Although *We* is a suitable measure of elasticity in a fluid, is a function of velocity, and thus not a proper elastic parameter.

Xanthan solutions, although normal stresses are very small, also present a relaxation time related to the orientation of polymer molecules in shearing flows. This relaxation time (according to rigid dumbbell theory) [33], is about 0.1–1 s in our case. Deborah number for these solutions is again less than unity and

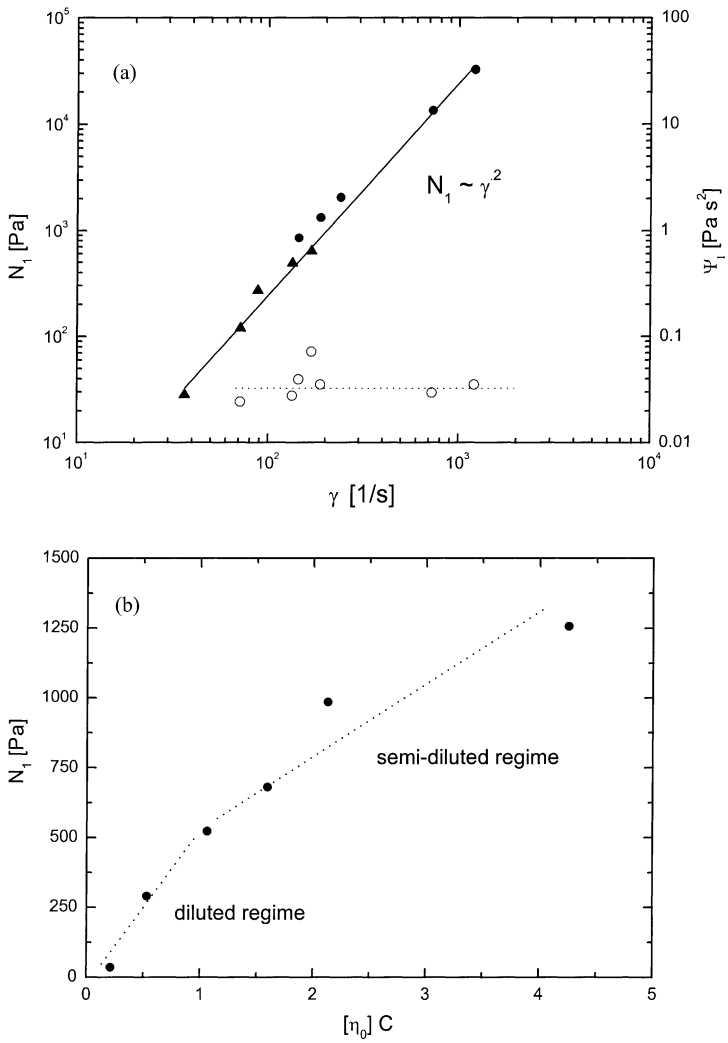

Fig. 4. (a) Log–log plot of the first normal stress difference N_1 vs. the shear rate $\dot{\gamma}$ for PAAm solution at $C = 2000$ ppm. Low shear measurements (▲) correspond to cone-plate measurements, high shear data (●) to die swell experiments. Hollow symbols represent first normal stress coefficient Ψ_1, which remains almost constant over a wide range of shear rates (∼0.03); (b) evolution of N_1 vs. the PAAm reduced concentration $[\eta_0]C$ for a shear rate of 200 s^{-1} ($[\eta_0] = 2.1 \times 10^{-2}$ wppm^{-1}). The lines shows the behavior above and below semi-dilute limit.

for that reason effective viscosity has no significant memory effect, at least at the angular velocities at which experiments were conducted.

3.3. Surface tension

Surface tension of solutions used in this work was also measured, since polymer concentration could possibly modify the interfacial properties, which play an important role in the construction of the parameter *Ca*. Surface tension was tested using the ring method with a Krüss K8 analog tensiometer. The results are

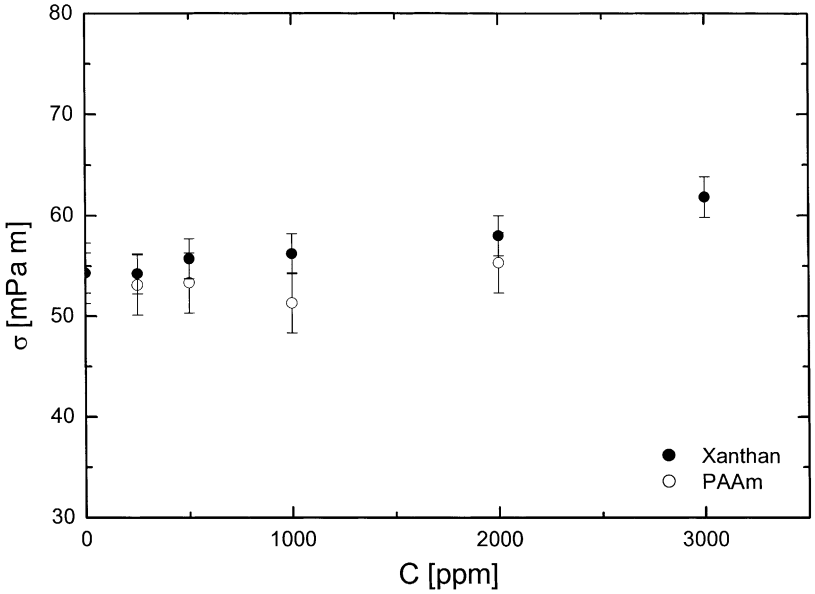

Fig. 5. Evolution of the surface tension of the solutions vs. concentration *C*.

shown as a function of polymer concentration in Fig. 5 for both fluids. First note the important reduction in surface tension, at concentration zero, with respect to tabulated values: while for a glycerol/water (85/15) solution at 23 °C a 64 mN/m value should be expected, a value of 54 mN/m was obtained for fluid extracted from the experiment. This decrease may be due to contamination of the water-based solution in the setup during experiments. Nevertheless, this value remained constant for all samples during the experiments conducted. Xanthan presents a slight increase in surface tension with concentration, possibly due to the ionic nature of this polymer [34]. While for inelastic solutions the ring method presents no difficulties, great care was taken while testing PAAm, since elongational effects may shadow the interfacial forces acting on the ring. For that reason, measurements were taken after transient effects were damped by viscosity. Nevertheless, results are scattered around solvent value $\sigma = 54 \pm 2$ mN/m and no distinguishable behavior can be asserted.

In both cases, since surface tension depends only slightly on concentration, we will neglect dynamic interfacial effects in the *Ca* evaluation. Therefore, it will be assumed that surface tension remains constant ($\sigma = 54$ mN/m) even if the amount of surface present below and above the instability threshold is not the same. Aging as well as dynamic effects on surface tension for these polymeric solutions have been studied in [35].

4. Results on instability threshold and beyond

4.1. Geometrical aspects: Ca versus aspect ratio*

In this section we present the experimental results obtained for the destabilization of the air–liquid interface as a function of geometrical parameters and polymer concentration. First, however, a comment

about how data is plotted in non-dimensional form must be stated. Usually, ribbing instability threshold is presented by plotting Ca^* versus geometrical parameters of the system, the most used is the aspect ratio of the system, $\Gamma = b_0/R$ [24]. In this way, all data can be plotted in non-dimensional form. The problem arises here when one attempts to define capillary number. Viscosity is a function of local shear rate (as $De \ll 1$ we will neglect history effects), and since journal-bearing flow is not strictly viscometric, the determination of viscosity in this experiment, and hence a correct evaluation of bulk forces, is not trivial a priori. As a first order estimate, it is assumed that the effective shear rate equals a pure Couette flow at the minimum thickness of the cell:

$$\dot{\gamma}_{\text{eff}} = \frac{V_\text{i} - V_\text{o}}{b} \approx \frac{V_\text{i}}{b}, \tag{5}$$

where V_i and V_o are the velocities of the inner and outer cylinders, respectively. As $V_\text{o} \ll V_\text{i}$ as explained in Section 2, it will be neglected in the following. This estimation of effective shear rate is accurate in the gap in the case of Couette-dominated flows, i.e. when pressure gradient effects are less important than shear effects due to boundaries. It is clearly not appropriate when cylinders rotate at the same velocity in the same direction [36] (in such a case the flow is Poiseuille-dominated, and it is then possible to estimate a mean shear rate as is done for power-law fluids flowing in Hele-Shaw cells [37,38]). A more physical evaluation of $\dot{\gamma}_{\text{eff}}$ would be to do the estimation at the meniscus position, but its position at threshold varies for each liquid. However, looking at the scales involved in our experiments, the flow might be considered viscometric since shear rate is only reduced by a factor two near meniscus position. The subsequent increase in viscosity is not significant near critical condition. Finally, evaluating $\mu(\dot{\gamma}_{\text{eff}})$ via Eq. (5), and assuming a constant surface tension, an effective capillary number can be expressed as

$$Ca_{\text{eff}} = \mu(\dot{\gamma}_{\text{eff}})\frac{V_\text{i}}{\sigma}. \tag{6}$$

In the following, we shall drop the index in Ca for simplicity. In this way, data for the onset versus the aspect ratio obtained in different configurations for non-Newtonian fluids can be compared with Newtonian results using a log–log representation (Fig. 6a). Data obtained from inelastic solutions, show no strong difference with respect to Newtonian behavior, even for high polymer concentration (2000 wppm), at which shear-dependent viscosity has a very important effect. For the case of PAAm solutions, a strong reduction on instability threshold is found. Assuming a linear dependence on aspect ratio $Ca^* \propto \Gamma$, proportionality constant drops from the Newtonian value of 38 to a value 4 for PAAm.

For comparison purpose, data obtained by other authors is plotted in Fig. 6b. Note that the results of Grillet et al. [21] as well as Bauman et al. [18] correspond to higher aspect ratios (10^{-2} to 10^{-1}), while Coyle et al. [24], and Dontula et al. [20] actually overlap our results. Nevertheless, all this data evidences the strong destabilizing effect of viscoelasticity.

4.2. Effect of polymer concentration: Ca^* versus C

The results shown in Section 4.1 highlight the strong influence of flexible polymers on threshold instability. For this reason, it is important to investigate the effect of concentration of polymer, especially for the viscoelastic case, and to determine the transition from highly concentrated solution to the Newtonian case. The gap was fixed at $b_0 = 0.4$ mm and thus the geometrical aspect ratio at $\Gamma = 4.12 \times 10^{-3}$ (value indicated by a vertical dashed line in Fig. 6) and concentration varied from 0 up to 2000 wppm for both polymers. The concentrations are reduced to intrinsic viscosity $[\eta_0]$, as defined in Section 3.

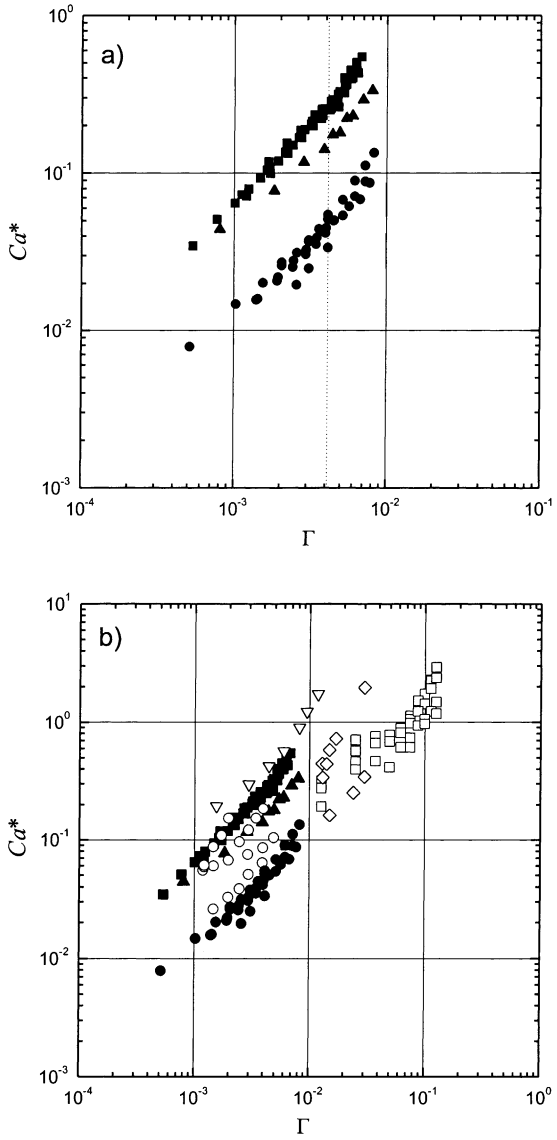

Fig. 6. (a) Log–log plot of the threshold value Ca^* vs. the aspect ratio of the cell Γ. (■) Newtonian solvent; (▲) Xanthan solution 2000 ppm; (●) PAAm solution 3000 ppm. Dotted vertical line corresponds to $\Gamma = 4.12 \times 10^{-3}$, the value at which critical Ca^* vs. polymer concentration has been measured (Fig. 7); (b) comparison between our data (filled symbols) and (□) [21]; (○) [20]; (◇) [18] and (▽) [24].

Determination of threshold has been conducted using the same technique as before (Section 2). Critical Ca is reduced to the Newtonian value $Ca^*_N = 0.175$. These results are presented in Fig. 7.

The results for Xanthan (Fig. 7a) show that in the dilute regime threshold remains almost constant at Newtonian value. Increasing C above the dilute regime generates a threshold drop which continues until it saturates at about 80% of Newtonian value. This saturation occurs at $[\eta_0]C \sim 2$ (300 wppm). It must be

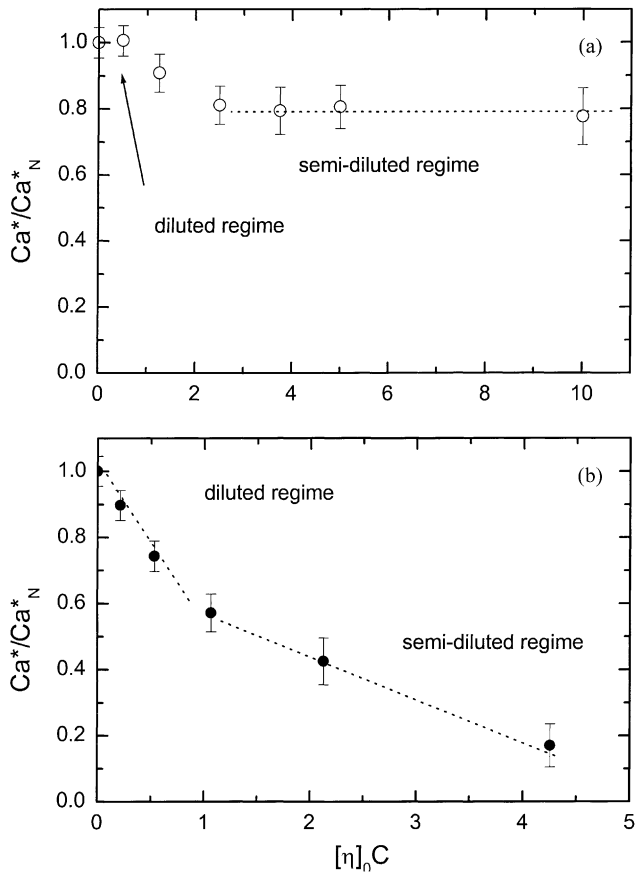

Fig. 7. Evolution of the threshold value Ca^* at $\Gamma = 4.12 \times 10^{-3}$ ($b_0 = 0.4$ mm) vs. the reduced concentration $[\eta_0]C$. (a) Xanthan solutions; (b) PAAm solutions.

noted that this effect is closely related to effective viscosity, since it is not above this concentration that shear-thinning effects are significant (at the shear rates involved near threshold). Velocities at threshold varied from 11 to 3 cm/s.

PAAm, on the other hand, behaves in a different way (Fig. 7b): threshold is monotonically reduced as concentration increases. This drop occurs even for the lowest concentrations. At higher concentrations, threshold is reduced, but less efficiently. On one hand, this might be correlated with the differences observed in normal stress measurements at low and high concentrations (Fig. 4b). On the other hand, as threshold is reduced, so does shear rate: velocity drops from 11 to 3 cm/s. As a consequence elastic effects become less effective and viscosity increases, overestimating Ca^*. Up to the concentrations explored, no saturation effect has been observed.

4.3. Amplitude of the wave forms near threshold

Above threshold, a regular pattern appears at the interface, as shown in Fig. 8, for different liquids. A detailed description of Newtonian finger shapes formed by ribbing instability can be found in [39].

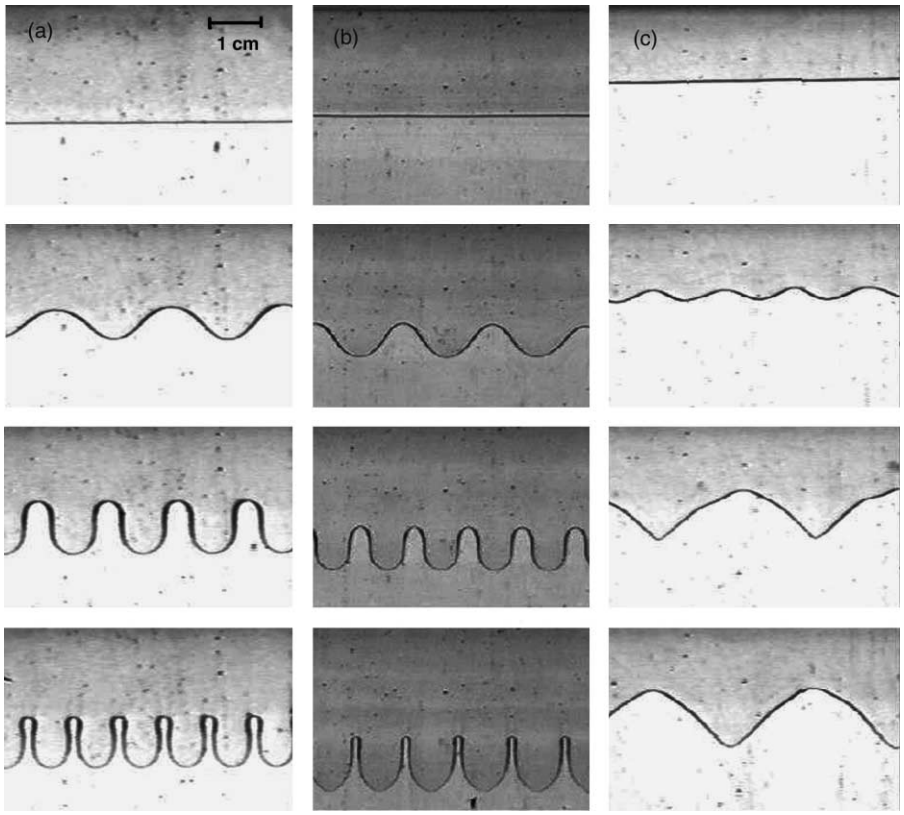

Fig. 8. Pictures of the interface below and above threshold (increasing *Ca* from up to down). On each picture, air is on the upper side. Minimum gap b_0 is exactly located at the lower boundary of each frame ($b_0 = 0.4$ mm). (a) Glycerol solution ($Ca = 0.210$, 0.226, 0.262, 0.425); (b) Xanthan 1000 wppm ($Ca = 0.076$, 0.123, 0.155, 0.338); (c) PAAm 1000 ppm ($Ca = 0.110$, 0.124, 0.154, 0.165).

In all cases, for *Ca* just above threshold, the shape of the interface is sinusoidal, regardless of rheological properties of the fluid. This is in agreement with non-linear single-mode Landau theory. Furthermore, the wavelength is comparable to Newtonian case as well. Nevertheless, further development of the pattern shows a strong dependence on rheology that separates from Newtonian behavior. In the case of Xanthan, it is only at higher *Ca* values that a sharp-peaked structure appears at the air–liquid fingertip, while liquid walls remain almost unchanged (Fig. 8b). Amplitude of the fingers, as well as its wavelength, is quite similar to those obtained in the Newtonian case. For PAAm, a triangular, saw-toothed pattern appears as soon as *Ca* is increased above threshold (Fig. 8c). Both amplitude and wavelength are much greater than the ones obtained for inelastic liquids. This is reminiscent of the growth of viscoelastic Saffman–Taylor fingers reported recently by Lindner [38], due to normal stresses acting on the coated film. Similar saw-toothed films have been reported previously by Grillet et al. [21] with a viscoelastic fluid. Another important fact concerning threshold can be seen in Fig. 8. The first frame in each column corresponds to the meniscus at *Ca* slightly lower than Ca^*. While for Xanthan there is no significant change in position with respect to the Newtonian case, for PAAm the (stable) meniscus position near

threshold is shifted away near 40%, from the prescribed Newtonian value equal to 2.12 (in units of Λ) [40]. This is an evidence of the non-Newtonian effects on base flow. Indeed, this meniscus displacement can be related to normal forces, as in die swell phenomena. The effect of meniscus shift on threshold drop is not completely clear, but this effect could indicate a change on film thickness on the cylinder.

Amplitude near threshold was measured in all cases. In Fig. 9, amplitude, $\xi = A/\Lambda$ of the pattern for different concentrations is plotted as a function of *Ca* showing the differences obtained from inelastic and elastic solutions. In the inelastic case, it seems that amplitude follows the same tendency as Newtonian

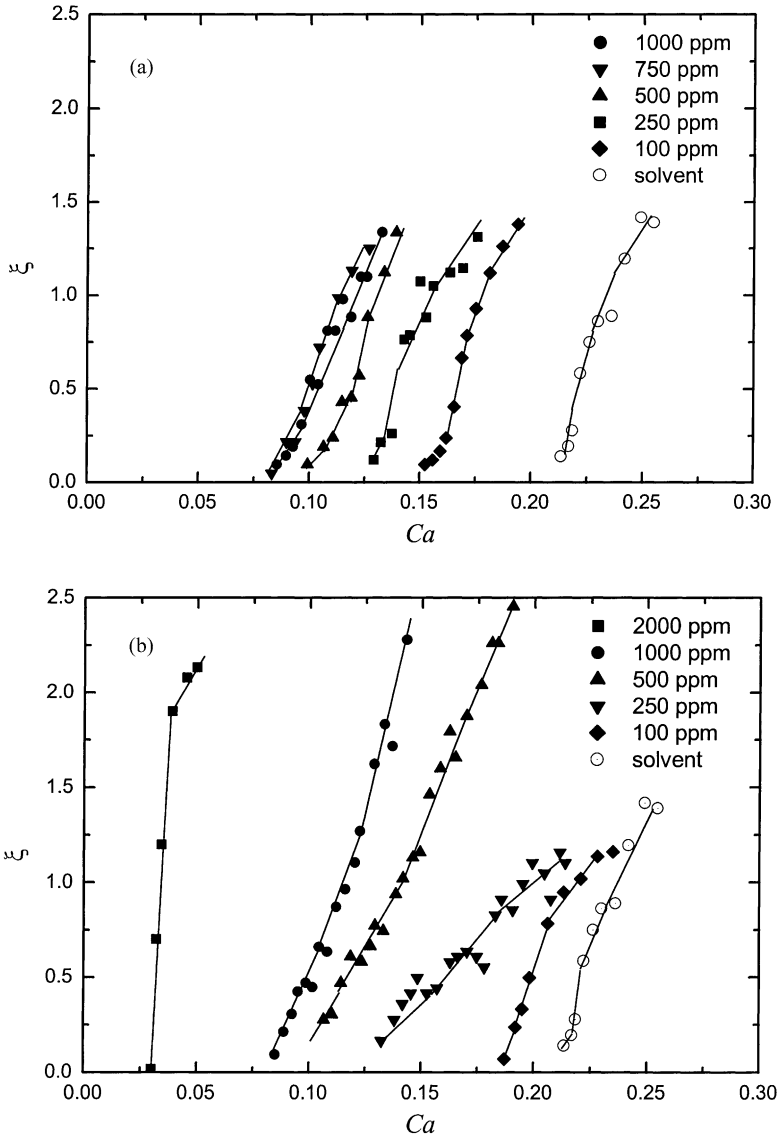

Fig. 9. Dimensionless amplitude of the wave form as a function of *Ca* (a) Xanthan; (b) PAAm. Hollow symbols represent Newtonian case.

case: amplitude growth and saturation remains similar. On the other hand, for PAAm solutions, these curves cannot be merged into a master curve by simply scaling *Ca* by the onset value Ca^*.

5. Discussion

In this work we reported the decrease of ribbing instability threshold, observed in non-Newtonian flows. It have been shown that shear-thinning solutions of Xanthan and PAAm were destabilized at a capillary number Ca^* lower than the value expected, even after first-order corrections on viscosity were made. In the case of inelastic solutions, this effect is directly related to effective viscosity. In the dilute regime, where shear-thinning effects are not measurable, no significant drop could be ascertained. It is only at higher concentration that a change in threshold conditions could be noticed. This effect can also be seen in Fig. 6a: as aspect ratio is reduced, from 10^{-2} to 10^{-3}, Ca^* approaches the Newtonian limit. This can be explained as follows: as aspect ratio is reduced, shear stresses become more important, shifting effective viscosity towards the Newtonian high-shear plateau. Viscosity gradients become less important throughout the nip, and the Newtonian result is retrieved. A correct evaluation of shear stresses through the nip near threshold, and the determination of the effect of viscosity differences near threshold will permit the introduction of second-order corrections to *Ca* in order to completely understand the effect of purely viscous non-Newtonian fluids on ribbing instability threshold.

The motivation for conducting the experiments shown in Fig. 7 was the spectacular threshold drop observed in the case of viscoelastic fluids, at a relatively high polymer concentration, shown in Fig. 6. Previous results of Bauman et al. [18] suggested that this occur even at low concentrations. Our results confirm this, since a significant threshold reduction occurs at concentrations lower than the semi-dilute limit. Above this, Ca^* values keeps reducing at a smaller rate, showing that the increase in polymer concentration in the semi-dilute regime introduces non-linearities in the behavior of the polymer solution under shear. The complexities arising from this coupling between effective viscosity and normal stresses was pointed out early by Greener and Middleman [14] in the case of film thickness determination. This is put in evidence in Fig. 4b, where first normal stress N_1 behaves distinctly above and below the semi-dilute limit. This provides evidence that first normal stress difference N_1 is behind the mechanism of elastic ribbing instability. If this is the case, it is clear that capillary number would be no longer the correct control parameter of this instability, and thus the onset could not collapse on a single Ca^*–Γ master curve.

There is not a common sense about the reason for such destabilizing effect. Bauman et al. [18] ascribed the decrease of onset for viscoelastic fluids to elongational viscosity effects in the bulk of the solution, while other authors (Ro and Homsy [16]) found similar behaviors when only normal stress effects at the interface are taken into account. More recent experimental results are in agreement with our results concerning the influence of geometrical aspects, even working at very different geometries under varying conditions, as can be seen in Fig. 6b. Dontula et al. [20] underestimate the role of elongational viscosity on ribbing threshold, formerly reported by Fernando and Glass [19] as a cause for the change on ribbing pattern in forward roll coating. There is very few predictions on wavelength at threshold. We did not observe a significant increase in wave number as reported in there work. Grillet et al. [21] found some evidence that elongational effects are responsible for the changes in shape, similar to the one shown in Fig. 8. In their work an elastic parameter *N*, defined as the ratio of *We*/*Ca* is defined to quantify the elastic effects present. Unfortunately, in our case shear thinning effects makes this definition rather cumbersome, since it becomes a function of velocity.

To clarify the physical origin of the efficiency of elasticity in decreasing the onset, more theoretical and experimental studies are necessary. Meniscus position near threshold, as well as film thickness on the walls, plays an important role in its determination, since it is closely related to the boundary conditions at the interface. In the Newtonian case, the meniscus position is determined from a balance between the incoming flux in the gap and the outcoming flux at the walls. The change in meniscus position observed in viscoelastic fluids must be related in some way to the threshold drop observed in these systems, both being due in part to elongational effects near stagnation lines or to normal stresses preventing the interface to recede further upstream. Experimentally the study of the position of the downstream meniscus below and at threshold for various concentrations and fluid nature could thus give valuable information on the basic flow and on normal stress effects at the interface. Moreover, the study of the critical capillary numbers when both cylinders rotate (already well documented for Newtonian fluids [6,36]) could be another fruitful way of investigation.

Acknowledgements

The authors wish to thank C. Allain for fruitful discussions on rheological aspects of solutions and its preparation and P. Perrot for die swell measurements. F.V.L. wishes to thank SIDERAR SA and Academia Nacional de Ciencias Exactas, Físicas y Naturales de Argentina for its financial support. This work is held with the support of the international cooperation program ECOS no. A97 E03 and PICS (CNRS-CONICET) no. 561.

References

[1] J.R.A. Pearson, The instability of uniform flow under roller and spreaders, J. Fluid Mech. 7 (1960) 481–500.
[2] E. Pitts, J. Greiller, The flow of liquid thin films between rollers, J. Fluid Mech. 11 (1961) 33–50.
[3] C.C. Mill, G.R. South, Formation of ribs on rotating rollers, J. Fluid Mech. 28 (1967) 523–529.
[4] K.J. Ruschak, Coating flows, Ann. Rev. Fluid Mech. 17 (1985) 65.
[5] M.D. Savage, Mathematical model for the onset of ribbing, AIChE J. 30 (1984) 999–1002.
[6] L. Bellon, L. Fourtune, V. Ter Minassian, M. Rabaud, Wave number selection and parity-breaking bifurcation in directional viscous fingering, Phys. Rev. E 58 (1998) 565–574.
[7] D.C.-H. Chen, in: N. Cheremisinoff (Ed.), Encyclopedia of Fluid Mechanics: A Review of the Role of Rheology in Coating Processes, Vol. 9, 1994, pp. 301–347.
[8] A. Beris, R.C. Armstrong, R.C. Brown, Perturbation theory for viscoelastic fluids between eccentric rotating cylinders, J. Non-Newtonian Fluid Mech. 13 (1983) 109–148.
[9] M.J. Davies, K. Walters, in: T.C. Davenport (Ed.), Rheology of Lubricants, Applied Science Publishers, Barking, p. 65.
[10] N. Phan-Thien, R.I. Tanner, Journal lubrication and normal stress measurements, J. Non-Newtonian Fluid Mech. 9 (1981) 107–117.
[11] P. Sinha, C. Singh, Lubrication of a cylinder on a plane with a non-Newtonian fluid considering cavitation, Trans. ASME 104 (1982) 168–172.
[12] I.K. Dien, H.G. Elrod, A generalized steady-state Reynolds equation for non-Newtonian fluids, with application to journal bearings, ASME J. Lubric. Tech. 105 (1983) 385–390.
[13] M.W. Johnson Jr., S. Mangkoesoebroto, Analysis of lubrication theory for the power law fluid, J. Tribol. 115 (1993) 71–77.
[14] Y. Greener, S. Middleman, A theory of roll coating of viscous and viscoelastic fluids, Polym. Eng. Sci. 15 (1975) 1–10.
[15] D.J. Coyle, C.W. Macosko, L.E. Scrive, Film-splitting flows of shear-thinning liquids in forward roll coating, AIChE J. 33 (5) (1987) 741–746.
[16] J.S. Ro, G.M. Homsy, Stability of viscoelastic interfacial flows between non-parallel walls: the ribbing instability of viscoelastic coating flows, 1998 (unpublished result).

[17] H. Benkreira, M.F. Edwards, W.L. Wilkinson, Roll coating of purely viscous liquids, Chem. Eng. Sci. 36 (1981) 429–434.
[18] T. Baumann, T. Sullivan, S. Middleman, Ribbing instability in coating flows: effect of polymer additives, Chem. Eng. Commun. 14 (1982) 35–46.
[19] R.H. Fernando, J.E. Glass, Dynamic uniaxial extensional viscosity (DUEV): effects in roll application. II. Polymer blend studies, J. Rheol. 32 (1982) 199–213.
[20] P. Dontula, M. Pasquali, C.W. Macosko, L.E. Scriven, Viscoelastic effects in forward-roll coating, in: A. Aït-Kadi, J.M. Dealy, D.F. James, M.C. Williams (Eds.), Proceedings of the XIIth International Congress on Rheology, Quebec City, Quebec, Canada 1996, pp. 709–710.
[21] A.M. Grillet, A.G. Lee, E.S.G. Shaqfeh, The stability of elastic fluid interfaces in coating flows, J. Fluid Mech. 399 (1999) 49–83.
[22] S. Michalland, M. Rabaud, Y. Couder, Instabilities of the upstream meniscus in directional viscous fingering, J. Fluid Mech. 312 (1996) 125–148.
[23] H.Z. Cummins, L. Fourtune, M. Rabaud, Successive bifurcations in directional viscous fingering, Phys. Rev. E 47 (1993) 1727–1738.
[24] D.J. Coyle, C.W. Macosko, L.E. Scriven, Stability of symmetric film-splitting between counter-rotating cylinders, J. Fluid Mech. 216 (1990) 437–458.
[25] P.G. Drazin, W.H. Reid, Hydrodynamic Stability, Cambridge University Press, Cambridge, 1982, p. 272.
[26] B. Tinland, M. Rinaudo, Dependence of the stiffness of the Xanthan chain on the external salt concentration, Macromolecules 22 (1989) 1863–1865.
[27] R.I. Tanner, Engineering Rheology, Oxford Science, Oxford, 1985.
[28] R. Byron Bird, R.C. Armstrong, O. Hassager, Dynamics of Polymeric Liquids, Vol. 1, Wiley, New York, 1987, p. 171.
[29] H. Fujita, Polymer Solutions, Elsevier, Amsterdam, 1990.
[30] C. Allain, M. Cloitre, P. Perrot, Experimental investigation and scaling law analysis of die swell in semi-dilute polymer solutions, J. Non-Newtonian Fluid Mech. 73 (1997) 51–66.
[31] L. Pauchard, F. Varela López, M. Rosen, C. Allain, P. Perrot, M. Rabaud, On the effects of non-Newtonian fluids above the ribbing instability, in: F. Durst, H. Raszillier (Eds.), Advances in Coating and Drying of Thin Films, Shaker, Aachen, 1999, pp. 183–188.
[32] G. Astarita, G. Marucci, Principles of Non-Newtonian Fluid Mechanics, McGraw Hill, London, 1974, p. 217.
[33] M.A. Zirnsak, D.V. Boger, V. Tirtaatmadja, Steady shear and dynamic rheological properties of Xanthan gum solutions in viscous solvents, J. Rheol. 43 (1999) 627–650.
[34] A.W. Adamson, A. Gast, Physical Chemistry of Surfaces, 6th Edition, Wiley, New York, 1997.
[35] R.K. Prud'homme, R.E. Long, Surface tensions of concentrated Xanthan and polyacrylamide solutions with added surfactants, J. Coll. Int. Sci. 93 (1983) 274–276.
[36] F. Varela López, L. Pauchard, M. Rosen, M. Rabaud, Threshold of ribbing instability with non-Newtonian fluids, in: F. Durst, H. Raszillier (Eds.), Advances in Coating and Drying of Thin Films, Shaker, Aachen, 1999, pp. 177–182.
[37] S. Obernauer, G. Drazer, M. Rosen, Stable unstable crossover in non-Newtonian radial Hele–Shaw flow, Physica A 283 (2000) 187–192.
[38] A. Lindner, L'instabilité de Saffman–Taylor dans les fluides complexes: relation entre les propriétés rheologiques et la formation de motifs, Thèse de doctorat de l'Université Paris VI, 2000.
[39] M. Rabaud, V. Hakim, Shape of stationary and travelling cells in the printer's instability, in: V. Chile, E. Tirapegui, W. Zeller (Eds.), Proceedings of the 3rd International Workshop on Instabilities and Non-Equilibrium Structures, Kluwer Academic Publishers, Dordrecht, 1989.
[40] D.A. Reinelt, The primary and inverse instabilities of directional viscous fingering, J. Fluid Mech. 285 (1995) 303–327.